Selective X-ray Bragg Spectrometry: Optimizing Fluorescence Microprobe Sensitivity for Precious Metals

B. Etschmann[1], C. Ryan[2], S. Vogt[3], J. Maser[3], M. Lintern[4], C. Harland[5], J. Brugger[6,7] and D. Legnini[3]

[1]CSIRO Exploration & Mining, Mineralogy, South Australian Museum, North Terrace, Adelaide, SA 5000, Australia
[2]CSIRO Exploration & Mining, School of Geosciences, Building 28E, Monash University, Clayton, VIC 3168, Australia
[3]Experimental Facilities Division, Advanced Photon Source, Argonne National Laboratory, 9700 S. Cass Ave, Argonne IL 60439 USA
[4]CSIRO Exploration & Mining, CRC LEME, 26 Dick Perry Ave. Kensington, WA 6151, Australia
[5]Australian Synchrotron Research Program (ANSTO), Advanced Photon Source, Argonne National Laboratory, 9700 S. Cass Ave, Argonne IL 60439 USA
[6]Mineralogy, South Australian Museum, North Terrace, Adelaide, SA 5000, Australia
[7]School of Earth and Environmental Sciences, University of Adelaide, Adelaide SA 5005, Australia

Introduction

Economic concentrations of gold in ore occur at the level of a few ppm, depending on ore mineralogy and the nature of gold residence in the ore. As the nature of gold residence affects the extraction techniques, there is much interest in the distribution of gold between coexisting sulphide minerals in ore which demands the imaging and analysis of gold at ppm to sub-ppm levels, at submicron spatial resolution. Similarly, thermodynamic data suggest that the concentration of gold in the fluids involved in ore formation in magmatic hydrothermal systems are seldomly higher than a few ppm. Hence, the study of ore fluids trapped and preserved as fluid inclusions in minerals necessitates the detection of gold at ppm to sub-ppm levels during in situ analysis of fluid inclusions. Gold anomalies in soils and calcrete are often in the range of 10's to 100' of ppb; knowledge of gold speciation in these fine grained samples is fundamental for understanding the origin of these anomalies, and in ranking different anomalies to select the most prospective exploration targets.

There is also a great interest in trace-element distributions in the biomedical sciences. For example, platinum in the form of cis-platin plays a major role in many chemotherapeutic drugs. Mapping and quantifying platinum distributions within tissues and single cells is therefore of great interest, e.g., to study the mode of action of chemotherapy drugs on tissues and cells on a sub-cellular level, as well as how these are altered in cells that develop resistivity against a specific drug. This knowledge could then be applied to the development and testing of new chemotherapeutic agents.

However, the very low concentration of precious metals, such as Au and Pt, in geological and biological samples challenges the detection sensitivity of high-resolution microanalytical probes. Destructive probes such as laser ablation can provide sensitive point analysis of geological material but only at low spatial resolution ($\geq$100 μm^2). SIMS can provide spatially resolved data at high sensitivity with some resolution compromise, but is difficult to quantify. Neither technique is well suited to delicate biological samples. Synchrotron X-ray fluorescence (SXRF) using a focused keV photon beam and proton induced X-ray emission (PIXE) using a focused MeV proton beam provide non-destructive analysis based on well characterized X-ray production mechanisms that lend themselves to standardless quantitative analysis, and real-time imaging capabilities with micron spatial resolution. Furthermore, these techniques permit the analysis and imaging of buried structures, such as fluid inclusions and microscopic precious metal minerals or individual cells in tissue or cultures. However, the concentration of precious metals often fall tantalizing below the detection limits of these techniques using conventional solid-state detection approaches. A major problem is the interference of other fluorescence lines with the lines that are to be detected. A distinguishing feature of SXRF is the possibility to use selective excitation of elements of interest,by tuning the incident X-ray energy. However, this only allows the elimination of elements with energetically higher absorption edges than the one to be studied. A major analytical interference for Au detection using L X-ray lines is the common association of Au with As in sulphide geological samples. Since the As K edge is lower in energy than the Au L edges, selective excitation cannot help in this case. Additionally, most geological samples contain large amounts of other elements that tend to fluoresce intensely. That not only increases the overall background level, but also results in a high count rate on the detector, with associated problems such as high dead time.

Similarly, in biological samples incomplete charge collection tailing from the scattered beam produces an elevated background which degrades ultimate detection sensitivity. Increasing the energy separation between Pt lines and beam energy in order to reduce tailing also reduces the ionisation cross-section nullifying any potential gain.

There are several approaches that can be used to address these problems: For example, Johansson double focussing crystal spectrometers based on Bragg diffraction offer high-energy resolution, which enable precious metal lines to be resolved from interferences. However, these spectrometers have low detection solid angles, which leads to low counting rates making them unsuitable for imaging applications. Similarly, high-resolution spectrometers based on microcalorimetry techniques have great potential for spectroscopy but lack high solid angle.

Advances in Bragg diffraction materials offer great potential to remedy this situation by permitting spectrometer designs combining selectivity with large effective solid angle. Techniques have been demonstrated for the fabrication of films of highly ordered pyrolytic graphite (HOPG) on surfaces of virtually arbitrary shape [1]. These techniques permit

construction of surfaces of <002> oriented HOPG with radii of curvature as small as 5 mm. Hence, surfaces can be designed for optical properties rather than for ease of fabrication. For example, the method has been applied to the construction of toroidal energy band-pass filters [2].

In 1914, de Broglie and Lindermann noted that the surface that provides an equal Bragg diffraction angle for all rays radiating from a point source follows a log-spiral curve [3]. The new HOPG techniques permit these surfaces to be fabricated and coated with ~200 μm of <002> oriented graphite. The broad mosaic spread of these films (~0.4º) also contributes to high peak reflection efficiencies (integrated reflectivity of ~0.2º) [1].

A recent approach using HOPG coated surfaces based on a log-spiral led to strong dispersion in the analyzed beam with diffracted photons detected using a pin-diode array [1,4], similar to log-spiral bent Laue crystal spectrometers. The present work utilizes an alternate geometry designed at the CSIRO that combines a log spiral surface of rotation with a focusing action similar to a toroidal analyzer to concentrate the selected photons into a solid-state detector (Fig. 1). The energy dispersive solid-state detector will provide further discrimination of interferences arising from scattered photons. The focusing effect leads to a large effective solid angle for photons satisfying the Bragg condition. The result is a simple Bragg Filter accessory for a solid-state detector, which combines rejection of unwanted lines and detector artifacts with efficient collection of signal from precious metals.

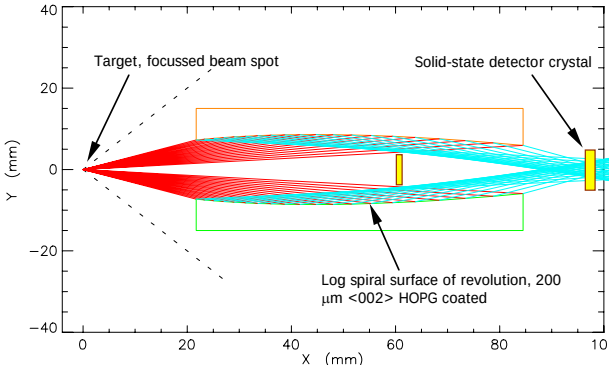

FIG 1: Ray tracing schematic of the cross-section of the Bragg Filter based on a log-spiral of revolution..

Methods and Materials

X-ray fluorescence data were collected at the 2-ID-E microprobe at the APS, using an incident beam energy of 12.1 keV. 2-ID-E is a branch beam-line that uses a silicon crystal beam splitter as a single bounce monochromator. X-rays were focused with a 20 cm Fresnel zone plate, resulting in a focused beam spot of ~1.3 μm. An order-sorting aperture intercepted higher diffraction orders and, in conjunction with a central stop, blocked the unfocussed beam. A single element Ge energy-dispersive detector was located at ~90° to minimize detection of the scattered beam. It was fitted with a conical collimator large enough to accept scattered X-rays from the Bragg Filter.

The Bragg Filter, located between the sample and the detector was placed on a motorized stage to allow the filter-sample distance to be optimized for a particular energy. The alignment of the filter was tuned by scanning the position of the filter (lateral and distance from the sample), and optimized by checking the intensity of the Au signal from a standard VFeAu foil (ratio of elements 13:7:80).

100 – 500 s line scans were collected on the NIST 1832/1833 standard foils, a NIST 610 standard glass, a polished sample of pyrite from the ore zone of the Emperor Mine, Fiji and a clay containing about 1ppm Au, with and without the filter.

Imaging was done by raster scanning the sample through the focused beam, and full spectra were acquired at each scan position. The clay sample was imaged with (~7 h) and without (~2 h) the filter. The Fiji pyrite sample was only imaged with the filter (~11 h), given that it had already been imaged previously (~7 h at 16.1 keV), without a filter.

Results and Discussion

Preliminary results, based on the line scans from the Fiji pyrite sample, demonstrate the filter response function, which was determined by plotting the ratio of peak areas with and without the filter (Fig. 2). This ratio shows an increase of ~4 at E ~ 9.7 keV. The Au $L_{\alpha 1}$ peak area was increased by a factor of 3.89. The As $K_{\alpha 1}$ peak area was also increased, but only by a factor of 1.18. Lines below an energy of 8.6 keV (Zn $K_{\alpha 1}$) were suppressed by an order of magnitude, while lines with an energy greater than 11.5 keV (Au $L_{\beta 2}$, As $K_{\beta}1$) were suppressed by a factor of 5. The Rayleigh beam scatter peak, which is visible as a small tail on the As $K_{\beta 1}$ peak in Fig. 3a, was suppressed on the spectrum collected with the filter (Fig. 3b). This filter response function was fitted with a Gaussian.

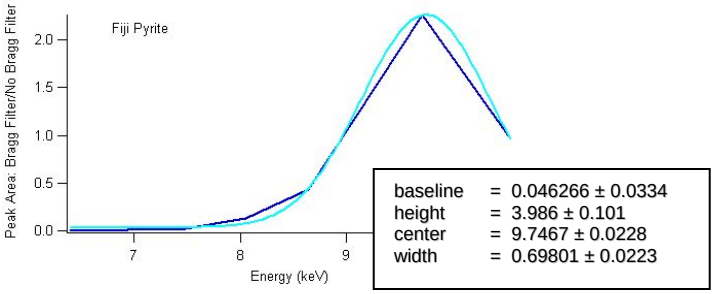

FIG 2: HOPG Bragg filter response function, showing the relative enhancement of X-rays of ~ 9.5keV.

However, a better fit was obtained with a skew Gaussian (width of 0.8 left of centroid and 1.4 above centroid). X-ray relative intensities calculated by GeoPIXE II [5,6] were multiplied by this response curve.

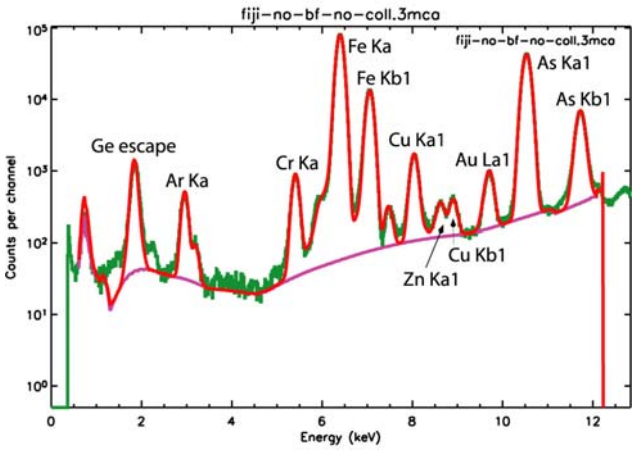

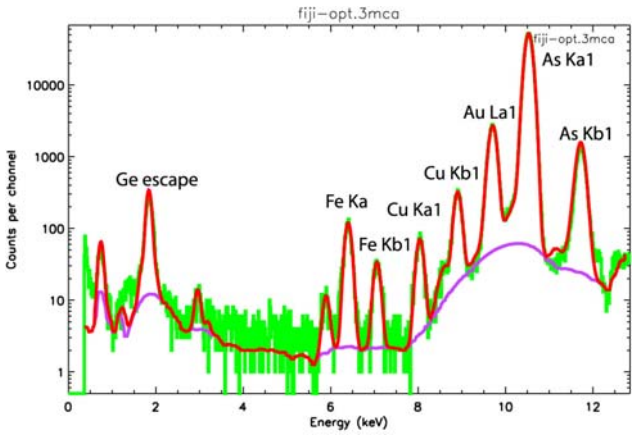

FIG 3: Fiji Pyrite spectrum – Top: collected without HOPG Bragg Filter, using "standard" X-ray relative intensities to fit the spectrum..Bottom: collected with HOPG Bragg Filter, using "standard" X-ray relative intensities multiplied by the skew Gaussian filter response function to fit the spectrum. Note the suppresion of X-rays outside the desired energy window.

The Fiji pyrite Au (L) images collected with (12.1 keV beam) and without (16.1 keV beam) the filter are compared in Fig. 4. The observed zonation using the Bragg Filter appears to show better definition. Not only do the trace-level Au zones appear more detailed in the image that was collected with the filter, an extra zone can be seen, highlighted by the green box.

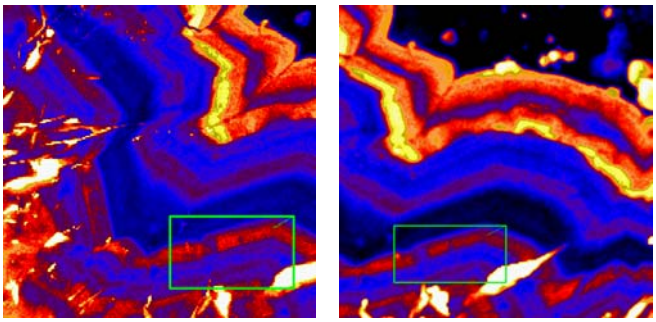

FIG 4: Image of Au (L) in Fiji Pyrite sample. Left: Imaged at 12.1 keV with the Bragg Filter in optimised position. Right: Imaged at 16.1 keV without the Bragg Filter. Maximum displayed concentrations of elements are: Fe ~ 45.4 wt%, Cu ~ 0.8 wt%, As ~ 3.5 wt% and Au ~ 0.4 wt%.

A similar Bragg filter response function was applied to fit the spectra of the clay sample (Fig. 5). A first-order approach to deal with the relatively sharp rise in the high energy end of the spectrum due to inelastically scattered beam was to change the baseline from a constant to a simple linear ramp (y=2.0*E + 0.5). More work is needed to properly account for the effects of the Bragg filter response on the continuum spectrum.

At these low Au concentrations, there are no Au peaks visible in the original spectrum. However, when Au was included in the refinement, the Au (L) image showed a concentrated hot-spot (as opposed to being evenly distributed throughout the clay). The spectrum extracted from this hotspot shows a Au (L) peak, which is more pronounced than in the spectrum collected without the filter.

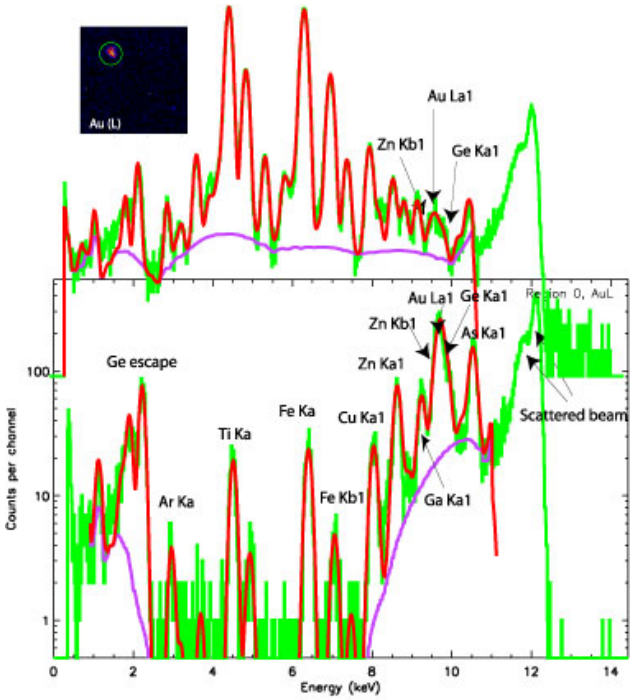

FIG 5: Clay sample with almost 1 ppm Au (average). Inset – Au image. Spectra are extracted from the region bounded by the green circle. Top – without the filter. Bottom – with the filter.

Conclusions

The HOPG Bragg Filter is relatively easy to use and align, and the use of the filter results in:

- Enhanced Au signal (~factor 4), and enhanced detection limits**.**
- Rejection of close interferences (e.g. As and scattered beam) together with their tails under the Au peak, further contributing to lower detection limits for Au.

Acknowledgements

This work was supported by the Australian Synchrotron Research Program, which is funded by the Commonwealth of Australia under the Major National Research Facilities Program. Use of the Advanced Photon Source was supported by the U.S. Department of Energy, Office of Science, Basic Energy Sciences, under Contract No. W-31-109-Eng-38.

References

[1] I.G. Grigorieva and A.A. Antonov. X-ray Spectrometry **32,** 64-68 (2003).

[2] Y. Kolmogorov and V. Trounova. X-ray Spectrometry **31,** 432-436 (2003).

[3] M. de Broglie and F.A. Lindemann. Compt. Rend. **158,** 944 (1914).

[4] D.M. Pease, M. Daniel and J.I. Budnik. Review Scientific Instrum**. 71**, 3267-3273 (2000).

[5] C.G. Ryan. "Quantitative Trace Element Imaging using PIXE and the Nuclear Microprobe" in *International Journal of Imaging Systems and Technology*, Special issue on "Advances in Quantitative Image Analysis", **11**, 219-230 (2000).

[6] GeoPIXE Software Package, http://nmp.csiro.au/GeoPIXE.html